Published September 26, 2014

Alteration of Biochar Carbon Chemistry during Soil Incubations: SR-FTIR and NEXAFS Investigation

Fungai N. D. Mukome
Dep. of Land, Air and Water Resources
Univ. of California
One Shields Ave.
Davis, CA 95616

Arthur L. D. Kilcoyne
Advanced Light Source
Lawrence Berkeley National Lab.
Berkeley, CA 94720

Sanjai J. Parikh*
Dep. of Land, Air and Water Resources
Univ. of California
One Shields Ave.
Davis, CA 95616

Near-edge X-ray absorption fine structure (NEXAFS) spectroscopy and synchrotron radiation based Fourier-transform infrared (SR-FTIR) microspectroscopy were utilized to systematically study the aging of three biochars under similar controlled conditions by tracking changes in the C chemistry of biochar in the presence and absence of a Typic Xerorthent soil. By utilizing both NEXAFS and SR-FTIR, differences in the initial biochar C functional group composition due to feedstock (aromatic C was greater in walnut shell biochar than softwood feedstock) and pyrolysis temperature (no long-range-ordered C in wood feedstock made at 410°C compared with 510°C) were confirmed. The data provided spectroscopic evidence corroborating both the conceptual biphasic model for biochar degradation and the power model of organic matter continuum mass loss as biochar ages due to a more labile aliphatic biochar portion and an aromatic portion that is oxidized more slowly. Incubations in the presence and absence of soil revealed a decrease in the ratio of the 287.6 eV peak (aliphatic C) relative to the 285.5 eV peak (aromatic C) during the incubations. Binding through functional groups present on the aged biochar surfaces (e.g., quinones, phenols, carbonyls) as well as the physical protection of the biochar by the soil appears to retard biochar surface decomposition. This study provides high-resolution spectroscopic data on discrete points on the biochar in addition to interactions between the soil and the biochar under conditions of minimal sample disturbance and destruction that corroborates current biochar stability and turnover models.

Abbreviations: NEXAFS, near-edge X-ray absorption fine structure; SR-FTIR, synchrotron radiation based Fourier-transform infrared; STXM, scanning transmission X-ray microscopy; XPS, X-ray photoelectron spectroscopy.

Biochar is a form of black carbon and is commonly defined as a product of biomass pyrolysis, or gasification, created for use as a beneficial soil amendment (Lehmann and Joseph, 2009). Biochar properties vary mainly according to feedstock and production temperature, but most biochars can be generally characterized as highly aromatic and significantly more resistant to microbial degradation than native soil C (Major et al., 2010; Spokas et al., 2009). Studies have demonstrated that biochar C turnover rates in soil are much slower than native soil C, and hence biochar has been proposed as a potential strategy for increasing terrestrial C through sequestration (Zimmerman, 2010).

Although a somewhat recalcitrant form of C, mineralization of biochar occurs with approximately equal contributions from both biotic and abiotic processes (Liang et al., 2006; Zimmerman, 2010). The main variables influencing the extent of biochar C mineralization are biochar pyrolysis temperature and feedstock, as well as soil conditions such as moisture content, temperature (Mukome et al., 2013b), and native soil organic matter (Cheng and Lehmann, 2009; Zimmerman

Supplemental material available online.
Soil Sci. Soc. Am. J. 78:1632–1640
doi:10.2136/sssaj2014.05.0206
Received 19 May 2014
*Corresponding author (sjparikh@ucdavis.edu).

et al., 2011). These factors impact the oxidation of biochar surfaces, as evidenced by higher O/C ratios on the exposed surfaces compared with the biochar interior (Brodowski et al., 2005).

Few studies have focused on the nanoscale organo–mineral interactions occurring at the soil–biochar or black carbon interface (Lin et al., 2012; Solomon et al., 2012). Lin et al. (2012), in a short-term (3-mo) incubation between two biochars and an Australian Ferrosol (soil with a high Fe oxide content and low-activity 1:1 clays), showed soil mineral incorporation on the biochar surface and suggested that Al^{3+} and Ca^{2+} may play a role in the soil–biochar interaction due to their abundance at the surface. They imaged the soil mineral–biochar interface using transmission electron microscopy and utilized X-ray photoelectron spectroscopy (XPS) to investigate the C bonding states in the biochar (Lin et al., 2012).

Biochar has been shown to undergo transformation as it ages, with several studies using different proxies, such as simulated geochemical weathering and ultraviolet oxidation, to investigate aging and oxidation effects on biochar stability (Skjernstad et al., 1999; Yao et al., 2010). However, these techniques, in addition to being destructive and not natural, were unable to resolve individual and specific interactions at the soil and biochar–soil mineral interface. As a result, the observed biochar transformations were inferred from changes in the bulk sample.

By utilizing high-level spatial resolution techniques, afforded by synchrotron radiation, we obtained data on discrete points of interaction between the soil and the biochar under conditions of minimal sample disturbance and destruction. Scanning transmission X-ray microscopy (STXM) has an analysis spot size of ~30 nm, compared with ~1 mm for XPS, and therefore affords the combination of energy and spatial resolution required to investigate in situ nanoscale variations of C forms (functional groups) in carbonaceous sources such as soil and biochar (Jacobsen et al., 2000; Scheinost et al., 2001). By scanning the photon energy through the absorption edge, (e.g., 285 eV for C) peak profiles are obtained that are characteristic for functional groups present in the sample, thereby giving rise to near-edge X-ray absorption fine structure (NEXAFS) spectra. Further, the excited states of the inner electron reflect the geometric and electronic structure of the molecule and can be correlated to the specific C functional groups present (Schafer et al., 2003; Stöhr, 1992). This feature makes STXM–NEXAFS a very sensitive technique to distinguish among aromatic C, phenol C, carbonyl C, aliphatic C, and carboxyl C with a resolution of only tens of nanometers and a useful tool for the determination of very fine heterogeneity of C in soil and other carbonaceous materials (Lehmann et al., 2005).

Additionally, our study benefited from the use of SR-FTIR analysis, which has previously been shown to be able to provide complementary data to STXM, corroborating specific chemical functional group interactions (Lehmann and Solomon, 2010). Synchrotron radiaiton based FTIR microspectroscopy has been used as a simple approach to track biogeochemical changes on the surfaces of environmental materials with high sensitivity and micrometer spatial resolution in real time (Holman and Martin, 2006; Schafer et al., 2003). Compared with conventional FTIR microspectroscopy, SR-FTIR microspectroscopy affords higher spatial resolution and higher accuracy and precision, good signal/noise ratios, and faster data collection (Yu et al., 2004).

The objective of this research was to systematically elucidate the aging of three biochars (made from two feedstocks: softwood and walnut shells) by investigating C chemistry transformations under similar controlled conditions in the presence and absence of a Typic Xerorthent soil with time (180 and 365 d).

MATERIALS AND METHODS

Soil and Biochars

Soil was collected from the surface horizon (Ap) in a walnut orchard (Winters, CA). The mapped soil series is Yolo (a fine-silty, mixed, nonacid, thermic Typic Xerorthent) and contains approximately 7% sand, 62% silt, and 31% clay (silty clay loam). The untreated soil was analyzed for total C and N with a C/N analyzer (Costech ECS 4010), for pH (1:2 w/v ratio with an equilibration time of 1 h) with an Orion 4 Star pH meter (Thermo Fisher Scientific), and for moisture content after drying for 24 h in an oven at 105°C. The study utilized two commercially available biochars, low-temperature (410°C) wood feedstock (WF_{410}) and high-temperature (510°C) wood feedstock (WF_{510}), and a third, high-temperature (900°C) walnut shell (WA_{900}) biochar obtained from a walnut processing facility. The wood biochars were made from a feedstock mixture of primarily Douglas fir [*Pseudotsuga menziesii* (Mirb.) Franco] with white fir [*Abies concolor* (Gordon & Glend.) Lindl. ex Hildebr.] in a slow pyrolysis process, and the walnut shell biochar was made from *Juglans californica* (S. Watson) walnut shells using a gasification process.

These biochars were selected based on the ability to compare very different feedstocks (softwood and walnut shells), the popularity of the feedstock for biochar production (wood), the ability to compare similar biochars made at different pyrolysis temperatures (WF_{410} and WF_{510}), and to represent the likely scenario where local biomass feedstocks will be used as a bioenergy source with a biochar byproduct available for soil amendment (walnut shell). For further details on the soil and biochar physical and chemical characteristics, as well as production conditions, see Mukome et al. (2013b).

Incubations

Biochar (0.5 g, <2 mm) was mixed into 50 g of air-dried soil for a 1.0% mixture (w/w), which equates to a typical field application rate of approximately 12 Mg ha^{-1} (using the top 10 cm for a field soil with a bulk density of 1.2 g cm^{-3}). Individual jars were considered experimental units in a randomized block design with an initial moisture content of 90% water-filled pore space (WFPS). The jars were then allowed to dry down, and a moisture content of 55 to 60% WFPS was maintained for the duration of the incubation. Treatments were conducted in triplicate, with destructive sampling occurring after 180 and 365 d. Incubations of biochar in the absence of soil were also performed

for similar lengths of time (no microbes added). For this, a similar amount of biochar (0.5 g) was maintained at the same water content as for the biochar–soil treatments. This study was a continuation of a prior study investigating the effect of these same biochar amendments on greenhouse gas emissions from this soil (Mukome et al., 2013a).

Preparation of Thin Sections

After the desired time intervals, subsamples of the soils (0.5 g) were frozen overnight at −70°C overnight and lyophilized (7 d). Biochar within the sample was manually selected using forceps (removed with intact surface interactions with soil where appropriate) and embedded in a sulfur block using a protocol modified from Hugo and Cady (2004). Specifically, in a fume hood, a blue silicone mold (Pelco 103, Ted Pella) with biochar samples in the microwells was placed on a hotplate (work surface temperature of 90–95°C). On a second hotplate, precipitated S (99.5–100.5% [w/w], Fisher Scientific) was melted on a stainless steel scoopula at 120°C. The molten S was carefully poured into individual microwells and allowed to equilibrate for a few minutes. A small S crystal on a needle was carefully just touched to the liquid droplet surface to nucleate solidification. This step was critical in producing a S capsule amenable to ultramicrotoming. Upon solidification, the S capsules were mounted onto resin capsules that could be fastened onto the ultramicrotome holder, with excess S removed using a glass knife. Thin sections were sliced using a diamond knife (Diatome) on a Leica Ultracut S ultramicrotome. Multiple thin sections were cut per sample, and at least two samples per treatment were analyzed. After sectioning, the thin sections were mounted onto Cu grids (200 mesh, no. 53002, Ladd Research) impregnated with silicon monoxide substrate. The grids were taped onto pinholes on Al sample plates designed for the STXM instrument. Residual S on the grids was removed by sublimation using a hotplate at 60°C for 15 min.

The NEXAFS spectra were collected on Beamline 5.3.2.2 at the Advanced Light Source, Lawrence Berkeley National Laboratory. Line scans and image scans (stacks) were acquired across the photon energies of the C K-edge (278–344 eV) to yield spectra after data analysis. A more detailed description of this instrument and its operation was provided by Kilcoyne et al. (2003). Post-processing of the data (stack aligning, principal component analysis, and clustering) was done using aXis2000 software and ATHENA software (spectral deconvolution) (Hitchcock, 2011; Ravel and Newville, 2005). Deconvolution was performed using an arctangent function for the ionization step at 290.5 eV (full width at half maximum set at 1 eV) and seven Gaussian peaks (284.3, 285.1, 286.1, 286.5, 287.2, 288. 2, and 289.3) with full width at half maximum set at 0.4 eV (see Table 1 for assignment). The spectra were initially pre-edge normalized to prevent spectral dependence on the total C content (Solomon et al., 2005). Only the discrete part of the spectra (284–290 eV) was utilized in the spectral deconvolution due to peak broadening and overlapping that occurs beyond 290 eV (Cody et al., 1998; Solomon et al., 2009). The sum total of the areas of arctangent function and the seven Gaussian peaks was set to 100% and the percentage contribution of each functional group determined (Table 1). The best fit for the spectra was obtained by not fixing the peak centroid.

The same thin sections were used for SR-FTIR analysis by a Thermo 670 Nicolet FTIR spectrophotometer on Beamline 1.4.4 at the Advanced Light Source, Lawrence Berkeley National Laboratory. The beamline is fitted with a Spectra Tech Continuum 32′ transmission, reflection microscope with a KBr splitter and Hg–Cd–Te detector that records spectra in the 600 to 7000 cm^{-1} region with a 1.0 cm^{-1} resolution. A total of 256 scans was collected per spectrum at a resolution of 4 cm^{-1}, and OMNIC ATLUS Version 8.0 (Thermo Nicolet Corp.) was utilized for spectral analysis. The spectra were baseline corrected and plotted after normalization to enable comparison.

The orientation of the thin sections sliced from the biochar enabled the observation of biochar–soil and biochar–soil–air space interfaces. The level of resolution also enabled spectra of the biochar to be collected at different distances from the biochar interfaces to investigate differences in C mineralization at the center of the biochar sample in comparison to the outer edge. The representative spectra attributed to the different individual materials (soil and biochar) were collected 1 mm from the biochar–soil interface.

RESULTS AND DISCUSSION

Effects of Feedstock and Pyrolysis Temperature on Biochar Chemical Composition

The NEXAFS spectra of the fresh biochar [Fig. 1(i), 2(i), and 3(i)] were generally consistent with soot and biochar edges observed in other studies (Brandes et al., 2004; Heymann et al., 2011; Kinyangi et al., 2006; Solomon et al., 2009). The wood feedstock biochars (WF_{410} and WF_{510}) had similar NEXAFS spectra, sharing three common peaks centered at approximately 285.5, 286.4, and 287.6 eV, as seen in Fig. 1(i) and 2(i). Differences arose in the peak at 285.5 eV (aromatic C), which was significantly larger in the WF_{510} than the WF_{410} spectra, and with the peak at 291.6 eV signifying long-range-ordered C absent in the lower temperature biochar. This is consistent with studies that have shown a higher pyrolysis production temperature to increase aromatic C relative to aliphatic C, resulting in biochar with greater aromatic structure (Heymann et al., 2011; Kloss et al., 2012; Van Zwieten et al., 2010). Both wood biochars had prominent peaks at approximately 287.4 eV due to the decomposition of cellulosic glycosyl units that yield several products including paraffinic compounds (Shafizadeh and Sekiguchi, 1984). The greater fraction of aliphatic C in the low-temperature biochar has been suggested to make such biochars more susceptible to microbial degradation (McBeath and Smernik, 2009). The effect of feedstock on the chemical composition was also evident in the difference between the wood feedstock biochars and the WA_{900} biochar. Although made at the highest temperature, the walnut shell biochar still had proportionally more aliphatic C than aromatic C. In addition, the

Table 1. Relative contributions of organic C functional groups estimated from C (1s) near-edge X-ray absorption fine structure spectra peak areas.

Sample	Quinone (284.3 eV)	Aromatic + olefinic (284.9–285.5 eV)	Phenolic (285.8–286.4 eV)	Ketonic (286.6 eV)	Aliphatic (287.1–287.5 eV)	Carbonyl + carboxylic (287.7–288.6 eV)	Alcohols (289.3–289.5 eV)	Aliphatic/aromatic	Oxidized C†
	%								
	Low-temperature (410°C) wood feedstock (WF_{410}) biochar								
Unincubated edge	–	–	–	4.69	24.47	15.52	16.39	–	31.92
Unincubated interior	–	4.35	–	5.17	26.01	16.07	12.53	5.97	28.61
180-d edge (no soil)	6.72	12.26	–	8.03	9.65	9.82	8.71	0.79	25.26
180-d interior (no soil)	–	16.44	7.78	–	13	11.38	11.12	0.79	30.28
365-d edge(no soil)	9.58	12.12	11.37	–	11.52	10.5	9.17	0.95	40.63
365-d interior (no soil)	10.75	15.32	11.365	14.35	10.36	8.41	3.63	0.68	34.43
180-d edge (in soil)	–	11.66	–	7.8	11.33	11.02	14.04	0.97	25.06
180-d interior (in soil)	–	11.96	–	–	12.16	9.19	17.11	1.02	26.3
365-d edge(in soil)	12.11	12.03	–	11.8	8.98	11.41	9.32	0.75	32.84
365-d interior (in soil)	13.35	14.52	9.86	–	10.2	8.81	7.74	0.7	39.76
	High-temperature (510°C) wood feedstock (WF_{510}) biochar								
Unincubated edge	9.85	17.39	9.26	–	12.32	8.9	6.27	0.71	34.28
Unincubated interior	9.59	16.36	13.1	9.12	13.69	8.24	4.15	–	35.07
180-d edge (no soil)	10.64	17.8	11.59		9.13	8.8	5.65	0.51	36.68
180-d interior (no soil)	8.58	17.33	15.91	10.6	8.89	8.37	5.51	0.51	38.37
365-d edge (no soil)	–	–	–	2.91	–	–	29.44	–	29.44
365-d interior (no soil)	–	–	–	2.21	–	–	28.87	–	28.87
180-d edge (in soil)	8.97	16.86	9.27	–	11.88	9.93	5.94	0.7	34.11
180-d interior (in soil)	9.02	13.81	10.2	–	11.51	7.59	6.51	0.83	33.31
365-d edge (in soil)	9.88	15.54	10.61	–	8.54	8.56	6.16	0.55	35.21
365-d interior (in soil)	11.3	17.12	11.77	–	10.98	9.42	6.6	0.64	39.1
	High-temperature (900°C) walnut shell (WA_{900}) biochar								
Unincubated edge	–	5.31	5.31	–	31.57	13.43	5.72	5.94	24.47
Unincubated interior	–	–	–	5.51	34.54	14.93	–	–	14.93
180-d edge (no soil)	–	17.16	9.27	–	12.73	11.46	6.04	0.74	26.78
180-d interior (no soil)	15.36	21.96	12.01	–	12.91	5.41	2.26	0.59	35.04
365-d edge (no soil)	8.91	16.45	12.78	8.86	11.29	8.67	5.66	0.69	36.02
365-d interior (no soil)	9.71	16.05	13.79	9.31	10.09	7.72	5.52	0.63	36.74
180-d edge (in soil)	8.66	14.38	9.66	–	13.32	11.5	9.75	0.93	39.56
180-d interior (in soil)	7.88	15.97	–	7.45	13.55	12.12	8.01	0.85	28.01
365-d edge (in soil)	8.73	12.53	9.36	–	11.52	10.5	6.87	0.92	35.46

† Oxidized C = quinone + phenolic + ketone + carbonyl + alcohol.

ratio of aliphatic C/aromatic C for WA_{900} was comparable to that of WF_{410}, a biochar made at a temperature 500°C lower.

Differences between the outer surface and interior C chemistry were not consistent for all the biochars and are only evident in the WF_{510} spectra [Fig. 2(i)]. The NEXAFS spectra of the exterior surfaces show increased functionalization, with added peaks at 289.3 and 290.3 eV. The increased C functional groups may arise from deposition of condensates of volatile compounds like polyaromatic hydrocarbons produced during pyrolysis (Spokas et al., 2011). These peaks have also been assigned to a series of "interlayer states" arising from stacking defects between the aromatic layers of graphite (Brandes et al., 2008).

The SR-FTIR spectra of the fresh (unincubated) biochars [Fig. 4(i), 5(i), and 6(i)] show a number of characteristic absorbance peaks. Peak assignments are presented in Supplemental Table S2. The conserved peaks observed in the two wood feedstock biochars were centered at 801 cm^{-1} (aromatic C–H), approximately 1020 cm^{-1} (aliphatic ether C–O and alcohol C–O), and approximately 1100 cm^{-1} (C–O–C esters). Biochar WF_{410} [Fig. 4(i)] exhibited greater functionalization than WF_{510} [Fig. 5(i)], which is consistent with the lower pyrolysis temperature of production of the former (Kim et al., 2011). The greater aromatic character observed in the NEXAFS spectra of WF_{510} was corroborated by the greater magnitude of aromatic C–H peaks (900–750 cm^{-1}) when comparing WF_{510} with WF_{410}.

The complementary information of the two synchrotron techniques is evidenced by their ability to qualitatively corroborate the presence of several functional groups including aromatic C–H, aliphatic C–H, carbonyl, and carboxylic C. The greater functionalization of the lower temperature biochar (WF_{410} compared with WF_{510}) is also consistent in both techniques.

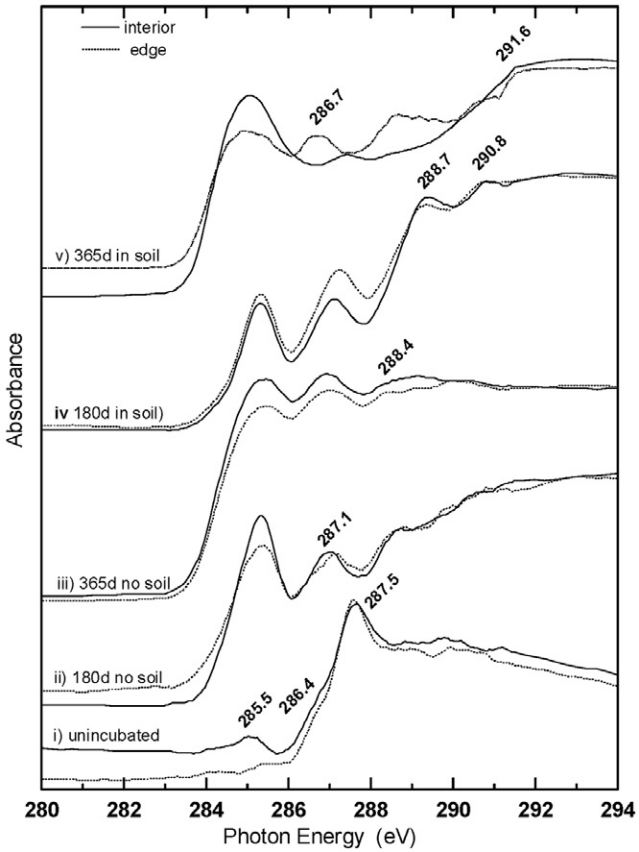

Fig. 1. Carbon (1s) near-edge X-ray absorption fine structure spectra of low-temperature (410°C) wood feedstock (WF_{410}) biochar unincubated (i), incubated in the absence of soil for 180 d (ii) and 365 d (iii), and incubated in the presence of soil for 180 d (iv) and 365 d (v).

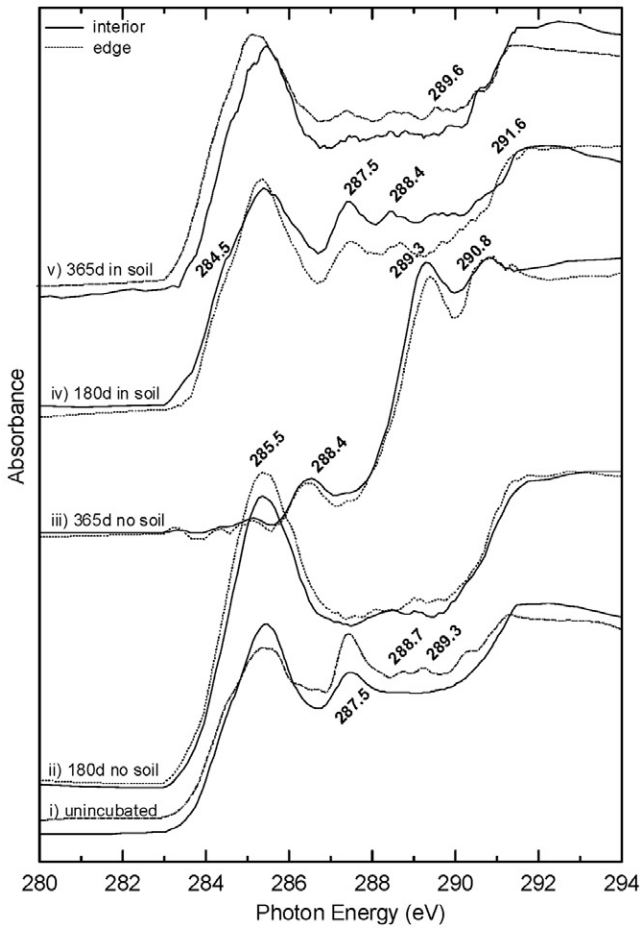

Fig. 2. Carbon (1s) near-edge X-ray absorption fine structure spectra of high-temperature (510°C) wood feedstock (WF_{510}) biochar unincubated (i), incubated in the absence of soil for 180 d (ii) and 365 d (iii), and incubated in the presence of soil for 180 d (iv) and 365 d (v).

Incubation Impacts on Black Carbon Chemistry

The C K-edge profiles show that the C chemistry of all three biochars was altered, with a trend toward increasing aromaticity after a year of incubation (Fig. 1–3). Deconvolution of the NEXAFS spectra show a semiquantitative change in the distribution of C functional groups. Although the results from deconvolution of the C K-edges are probably slight overestimates due to overlapping bands in the interpretation of the NEXAFS spectra, deconvolution of C K-edge NEXAFS spectra for other similar carbonaceous materials (humic and fulvic acids) have been shown to be well correlated to ^{13}C nuclear magnetic resonance spectroscopic data, providing precedence for the use of these data for semiquantitative interpretation of biochar (Schafer et al., 2003; Solomon et al., 2005). The major change consistent in all biochars is the deviation in the ratio of the 287.6 eV peak (aliphatic C) relative to the 285.5 eV peak (aromatic C) for the fresh biochar and the incubated biochars (both 180 and 365 d). The largest changes are for the WA_{900} and WF_{410} biochars, which decreased from approximately 5.9 to <1 (Table 1). This is consistent with a decrease in the contribution of the aliphatic C peak for all the biochars during the length of the incubation (Table 1).

In a 4-mo incubation of biochar at 30 and 70°C, a similar decrease in aliphatic C was observed and attributed to chemical oxidation of aliphatic C to C–O groups, soluble organic acids, and CO_2 (Cody and Alexander, 2005). Our results provide spectroscopic evidence for the conceptual biphasic model of biochar degradation proposed by Lehmann et al. (2009) comprising a labile aliphatic portion that is readily mineralized and an aromatic portion that is oxidized more slowly.

In contrast, Lin et al. (2012) observed a decrease in the relative content of the peak at approximately 285.0 eV (attributed to C–C/C–H and C=C) when comparing aged (3 mo) vs. fresh biochar made from poultry manure (with sawdust) and paper-mill sludge (with woodchips) using XPS data. An increase in the oxidized C forms (COOH, C–OH, and C=O) was also observed by Lin et al. (2012), whereas the biochars in the current study showed only a slight increase in the percentage of oxidized C (i.e., ~32–41% for WF_{410} edge) (Table 1) but an increase in the types of oxidized C. This observation is consistent with the slow oxidation of biochar. Further evidence for the oxidation of biochar C forms is a gradual shift to higher energy of the C=C 1s-π^* peak (centered at approximately 285.0 eV) as a function of the length of incubation. Similar shifts in C K-edges have been attributed to the presence of electron-withdrawing groups, such as O, being added to or substituted on the aromatic C=C structure (Moffet et al., 2010; Solomon et al., 2009).

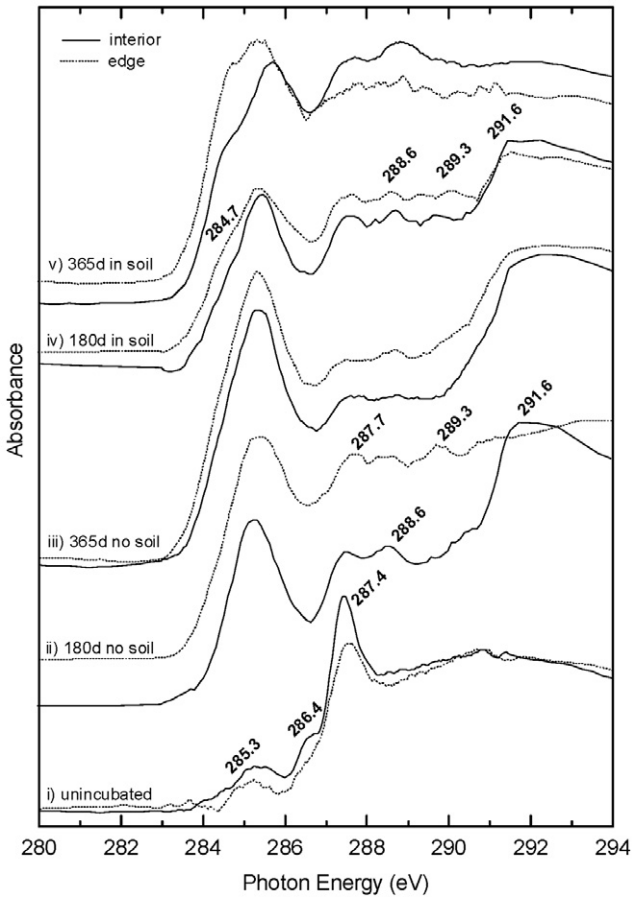

Fig. 3. Carbon (1s) near-edge X-ray absorption fine structure spectra of high-temperature (900°C) walnut shell (WA_{900}) biochar unincubated (i), incubated in the absence of soil for 180 d (ii) and 365 d (iii), and incubated in the presence of soil for 180 d (iv) and 365 d (v).

A potential proxy to gauge the oxidation (decomposition) of the biochar is the quinone shoulder peak (centered at approximately 284.3 eV). This peak is absent in the spectra

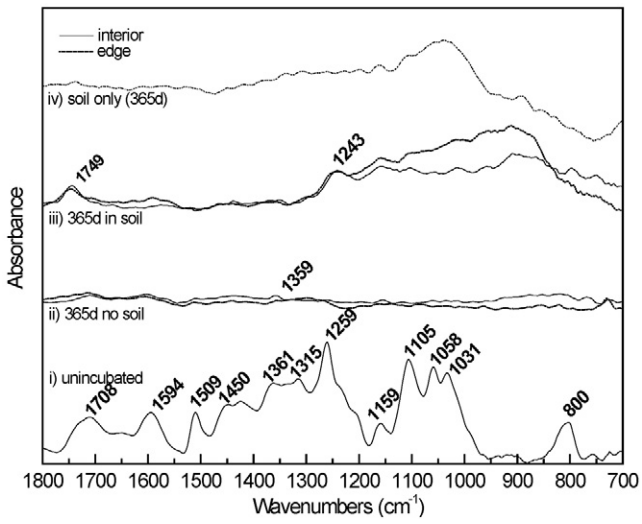

Fig. 4. Synchrotron radiation based Fourier-transform infrared spectra of unincubated low-temperature (410°C) wood feedstock (WF_{410}) biochar (i), WF_{410} biochar after incubation for 365 d in the absence of soil (ii), WF_{410} biochar after incubation for 365 d in the presence of soil (iii), and soil only after 365 d (iv).

of fresh WF_{410} and WA_{900} but accounts for approximately 10% of the total C after incubation (Fig. 1 and 3). The WF_{510} biochar had quinone C peaks before incubation, but after 365 d of incubation the peaks were absent. According to the polyphenol theory of humic substances formation, quinones are intermediates in the formation of humic acids from lignin and other non-lignin sources such as cellulose (Stevenson, 1994). The high gasification temperatures of the walnut shell biochar can account for the absence of quinone C peaks in the fresh WA_{900}.

The increase in quinone C, a redox active group, as the biochar ages is likely to have environmental ramifications on other matrices (e.g., soil and clay minerals) interacting with the biochar. Scott et al. (1998) were able to show that quinones in humic substances from a variety of environments were capable of accepting electrons in anoxic microbial respiration, suggesting that these moieties are the key reducible moiety within humic substances. Similarly, biochar may facilitate anaerobic oxidation of natural and xenobiotic organic compounds in contaminated soils and sediments (Lovley et al., 1996).

Our results could also be applicable to the biochar degradation mathematical model proposed by Zimmerman (2010), analogous to the organic matter "power model" that was used to explain organic matter decomposition in organic sediments (Middelburg, 1989). The power model proposes a continuum of mass loss starting with the labile (aliphatic) fraction and ending with a more refractory (aromatic condensed structure) fraction, and our SR-FTIR data support this assertion. The SR-FTIR spectra show a loss in infrared absorbance attributable to a reduction of polar functional groups and increased aromaticity [Fig. 4(i–ii), 5(i–ii), and 6(i–ii)]. The resultant aromatic condensed structure is a strong absorber of the infrared radiation like black carbon, and this results in poor spectra that are difficult to interpret due to the poor signal/noise ratio (Boehm, 1994). In addition, the few peaks that can be determined are broad, which, for biochar, has been attributed to the range of electronic environments about a given functional group (Donnet and Voet, 1976). Despite the decrease in functionality, the aged biochars show slight peaks that are consistent with aromatic carbonyls, such as quinones (1710–1750 cm^{-1}) and aromatic C=C (1590–1610 cm^{-1}) functional groups, corroborating the NEXAFS data.

The SR-FTIR spectra show no major differences in composition of the exposed and unexposed biochar surfaces except for WF_{510}, which shows small differences [Fig. 4(ii), 5(ii), and 6(ii)]. For the WF_{510} biochar [Fig. 5(ii)], the exposed surface of the biochar had a greater content of functional groups than the interior, with prominent peaks at approximately 1750, 1560, and 1260 cm^{-1}. These peaks are associated with aromatic carbonyl (quinones) and carboxyls, carboxylic acid C–O stretching, and carboxylic acid O–H deformation, respectively. This result was consistent with the NEXAFS spectra, which showed peaks associated with quinones (284.3 eV) and carbonyls (287.7–288.6eV) for these samples.

Soil Biochar Incubations

A considerable difference is observable between the biochars incubated in the presence and absence of soil [Fig. 1–3, (ii) vs. (iv) and (iii) vs. (v)], representative for all biochars studied. The presence of soil resulted in an increase in aromaticity of the biochar surfaces but with greater conservation or stabilization of the initial biochar surface functionality compared with conditions where the soil was absent. This is suggested by the greater prominence of aliphatic C peaks (centered at 287.1 eV) and the semiquantitative percentage estimates presented in Table 1. Further potential evidence is provided by the peak area ratio of the aliphatic C/aromatic C, which is greater for the soil-incubated samples than for the samples incubated without soil. For example, the aliphatic C/aromatic C ratio for the WF_{410} core is 0.97 (in soil) vs. 0.79 (no soil) after 180 d of incubation. A similar comparison was not possible for WF_{510} due to the absence of the comparative peaks in the samples incubated without soil. Greater preservation of the biochar surface C (content and distribution) after incubation in the presence of soil may be attributed to physical protection from microbial degradation. This is consistent with several other studies of biochar with and without soil, and several mechanisms for this have been proposed including occlusion in soil microaggregates, interactions with soil minerals, and sorption of organic matter (Brodowski et al., 2006; Liang et al., 2006).

Noticeable, particularly in the WF_{510} and WA_{900} NEXAFS spectra [Fig. 2(v) and 3(v)], is the shoulder peak at 284.3 eV (associated with the quinone C moiety) that increases with the duration of incubation. Our new finding of increased quinones on the biochar surface as a function of the duration of incubation corroborates the hypothesis presented by Briones (2012), who hypothesized that the addition of biochar and subsequent synergistic interaction with humic acids may account for the long-term success of sustainable soils such as Terra Preta or Amazon dark earth soils. Biochar does not afford an inert, stable, and high-surface-area matrix for bacteria to colonize, but rather it provides a site for biofilm formation (particularly for bacteria involved in extracellular electron transfer), with biochar surface quinones actively facilitating electron shuttling between the microbes and soil metal oxides under wet, anaerobic or anoxic conditions, as suggested by Briones (2012).

Briones (2012) further proposed that the role of functional groups on the biochar surface such as quinones provides a plausible explanation for mitigation of CH_4 mineralization of the biochar surface. Published results regarding microbial mineralization of biochar are ambiguous, some suggesting that the process can be microbially mediated (Bruun et al., 2008; Zimmerman, 2010) and others proposing an abiotically mediated process (Karhu et al., 2011; Liu et al., 2011). In our previous study of CO_2 and N_2O emissions from incubations of these three biochars with compost, the role of quinones on the surface of the WF_{510} and WA_{900} biochars may provide further explanation for the low N_2O emissions observed (Mukome et al., 2013a).

The samples incubated with soil also exhibited greater functionalization of the surface C as evidenced by a greater percentage of oxidized C (Table 1). The functionalization of the biochar surface may be due to mineralization. Published literature regarding microbial mineralization of biochar is ambiguous, with some findings suggesting that the process can be microbially mediated (Bruun et al., 2008; Zimmerman, 2010) and others proposing an abiotically mediated process (Cheng et al., 2006; Kaal et al., 2008). For example, comparing microbially inoculated and uninoculated black locust (*Robinia pseudoacacia* L.) bark biochar, Cheng et al. (2006) showed that microbial activity had no effect on the surface oxidation of biochar, suggesting abiotic processes as the mechanism of oxidation. Several types of reactions have been proposed for the weathering of biochar in soil: dissolution and precipitation, hydrolysis, carbonation and decarbonation, hydration, and redox reactions (Joseph et al., 2010). Surface functionalization has also been attributed to binding

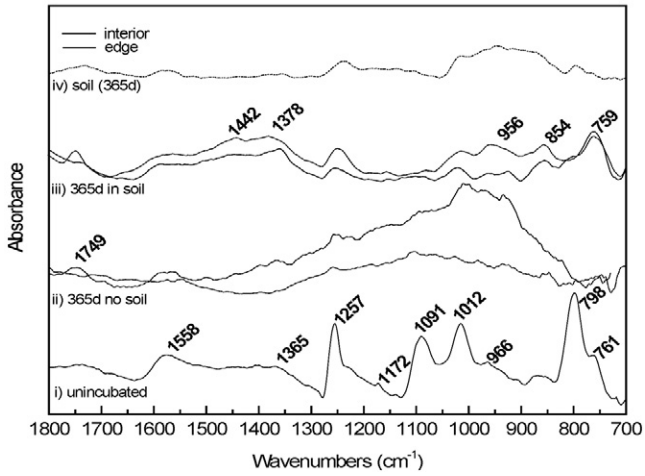

Fig. 5. Synchrotron radiation based Fourier-transform infrared spectra of unincubated high-temperature (510°C) wood feedstock (WF_{510}) biochar (i), WF_{410} biochar after incubation for 365 d in the absence of soil (ii), WF_{410} biochar after incubation for 365 d in the presence of soil (iii), and soil only after 365 d (iv).

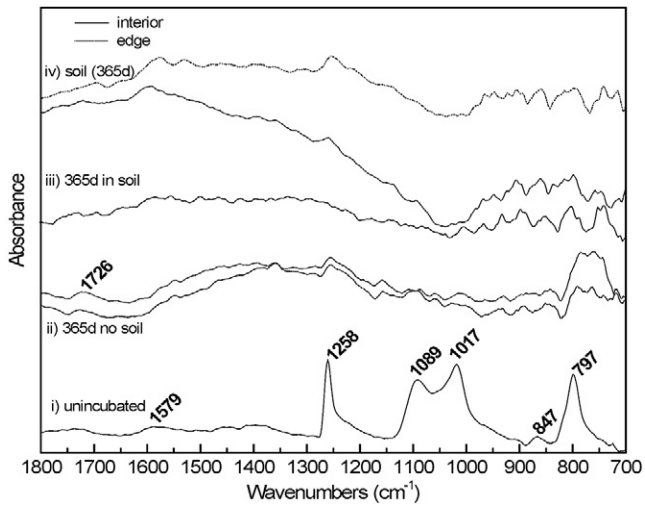

Fig. 6. Synchrotron radiation based Fourier-transform infrared spectra of unincubated high-temperature (900°C) walnut shell (WA_{900}) biochar (i), WF_{410} biochar after incubation for 365 d in the absence of soil (ii), WF_{410} biochar after incubation for 365 d in the presence of soil (iii), and soil only after 365 d (iv).

interactions with clay minerals and adsorption of organic matter onto the biochar (Uchimiya et al., 2010).

In a NEXAFS study of biochar particles from Amazon dark earth soils, Lehmann et al. (2005) observed highly aromatic biochar cores with a progressive oxidation of the region around the core (evidenced by carboxylic and phenolic C signatures). Organic matter such as microbial exudates are believed to form coatings on the surfaces (of biochar and soil) through rapid and irreversible van der Waals and H bonds (Chenu and Stotzky, 2002).

CONCLUSIONS

Scanning transmission X-ray microscopy and SR-FTIR were used to probe the biochar C chemistry at high spatial resolution, providing further evidence for current biochar stability and turnover models. The two techniques confirm differences in the initial biochar structure due to feedstock and pyrolysis temperature, and they provide spectroscopic evidence corroborating both the conceptual biphasic model for biochar degradation and the power model of organic matter continuum mass loss as biochar ages due to a more labile aliphatic biochar portion and an aromatic portion that is oxidized more slowly. Incubations in the presence and absence of soil revealed changes in C functional groups within the biochar as a function of time. This study contributes to our understanding of the processes controlling the chemical stabilization and in situ degradation (biological and chemical), which is critical for the development of soil–biochar management strategies and climate change models that incorporate biochar amendments. While our data set is not exhaustive, it does highlight the importance of considering biochar feedstock material and pyrolysis conditions before soil application of biochar. The effects of soil type and climate, not addressed in this study, are also expected to influence biochar stability and are important areas for future investigation.

SUPPLEMENTAL MATERIAL

Tables listing the NEXAFS and SR-FTIR peak assignments as well as the key physical and chemical properties of the study biochar are available in the online supplemental information. A figure showing the method utilized to determine representative spectra (obtained through principal component and clustering analysis) is also presented.

ACKNOWLEDGMENTS

We thank Emma Lee from the UC-Davis School of Medicine, Electron Microscopy Laboratory, for ultramicrotoming of the thin sections and Dr. Hans Betchel and Dr. Michael Martin for support at the Advanced Light Source (ALS) beamline 1.4.4. The Advanced Light Source is supported by the Director, Office of Science, Office of Basic Energy Sciences, of the USDOE under Contract no. DE-AC02-05CH11231. We also thank members the UC-Davis Parikh Environmental Chemistry Laboratory for assisting in analysis of samples at ALS. Funding was provided by the UC-Davis Agricultural Sustainability Institute (ASI) through a grant from the David and Lucile Packard Foundation, the USDA National Institute of Food and Agriculture (NIFA) through Hatch Formula Funding and multistate regional project W-2082, and the National Institute of Environmental Health Sciences (NIEHS) and National Institute of Health (NIH) through Grant 5 P42 ES0046599.

REFERENCES

Boehm, H.P. 1994. Some aspects of the surface chemistry of carbon blacks and other carbons. Carbon 32:759–769. doi:10.1016/0008-6223(94)90031-0

Brandes, J.A., G.D. Cody, D. Rumble, P. Haberstroh, S. Wirick, and Y. Gelinas. 2008. Carbon K-edge XANES spectromicroscopy of natural graphite. Carbon 46:1424–1434. doi:10.1016/j.carbon.2008.06.020

Brandes, J.A., C. Lee, S. Wakeham, M. Peterson, C. Jacobsen, S. Wirick, and G. Cody. 2004. Examining marine particulate organic matter at sub-micron scales using scanning transmission X-ray microscopy and carbon X-ray absorption near edge structure spectroscopy. Mar. Chem. 92:107–121. doi:10.1016/j.marchem.2004.06.020

Briones, A. 2012. The secrets of El Dorado viewed through a microbial perspective. Front. Microbiol. 2012(July). doi:10.3389/fmicb.2012.00239

Brodowski, S., W. Amelung, L. Haumaier, C. Abetz, and W. Zech. 2005. Morphological and chemical properties of black carbon in physical soil fractions as revealed by scanning electron microscopy and energy-dispersive X-ray spectroscopy. Geoderma 128:116–129. doi:10.1016/j.geoderma.2004.12.019

Brodowski, S., B. John, H. Flessa, and W. Amelung. 2006. Aggregate-occluded black carbon in soil. Eur. J. Soil Sci. 57:539–546. doi:10.1111/j.1365-2389.2006.00807.x

Bruun, S., E.S. Jensen, and L.S. Jensen. 2008. Microbial mineralization and assimilation of black carbon: Dependency on degree of thermal alteration. Org. Geochem. 39:839–845. doi:10.1016/j.orggeochem.2008.04.020

Cheng, C.-H., and J. Lehmann. 2009. Ageing of black carbon along a temperature gradient. Chemosphere 75:1021–1027. doi:10.1016/j.chemosphere.2009.01.045

Cheng, C.-H., J. Lehmann, J.E. Thies, S.D. Burton, and M.H. Engelhard. 2006. Oxidation of black carbon by biotic and abiotic processes. Org. Geochem. 37:1477–1488. doi:10.1016/j.orggeochem.2006.06.022

Chenu, C., and G. Stotzky. 2002. Interactions between microorganisms and soil particles: An overview. In: P.M. Huang et al., editors, Interactions between soil particles and microorganisms: Impact on the terrestrial ecosystem. John Wiley & Sons, Chichester, UK. p. 4–39.

Cody, G.D., H. Ade, S. Wirick, G.D. Mitchell, and A. Davis. 1998. Determination of chemical-structural changes in vitrinite accompanying luminescence alteration using C-NEXAFS analysis. Organic Geochemistry 28:441–455. doi:10.1016/S0146–6380(98)00010-2

Cody, G.D., and C.M.O.D. Alexander. 2005. NMR studies of chemical structural variation of insoluble organic matter from different carbonaceous chondrite groups. Geochim. Cosmochim. Acta 69:1085–1097. doi:10.1016/j.gca.2004.08.031

Donnet, J.B., and A. Voet. 1976. Carbon black: Physics, chemistry, and elastomer reinforcement. Marcel Dekker, New York.

Heymann, K., J. Lehmann, D. Solomon, M.W.I. Schmidt, and T. Regier. 2011. C 1s K-edge near edge X-ray absorption fine structure (NEXAFS) spectroscopy for characterizing functional group chemistry of black carbon. Org. Geochem. 42:1055–1064. doi:10.1016/j.orggeochem.2011.06.021

Hitchcock, A.P. 2011. aXis2000: Analysis of X-ray images and spectra. McMaster Univ., Hamilton, ON, Canada. http://unicorn.mcmaster.ca/aXis2000.html.

Holman, H.Y.N., and M.C. Martin. 2006. Synchrotron radiation infrared spectromicroscopy: A noninvasive chemical probe for monitoring biogeochemical processes. Adv. Agron. 90:79–127.

Hugo, R.C., and S.L. Cady. 2004. Preparation of geological and biological TEM specimens by embedding in sulfur. Microsc. Today 12:28–30.

Jacobsen, C., S. Wirick, G. Flynn, and C. Zimba. 2000. Soft X-ray spectroscopy from image sequences with sub-100 nm spatial resolution. J. Microsc. 197:173–184. doi:10.1046/j.1365-2818.2000.00640.x

Joseph, S.D., M. Camps-Arbestain, Y. Lin, P. Munroe, C.H. Chia, J. Hook, et al. 2010. An investigation into the reactions of biochar in soil. Aust. J. Soil Res. 48:501–515. doi:10.1071/SR10009

Kaal, J., S. Brodowski, J.A. Baldock, K.G.J. Nierop, and A.M. Cortizas. 2008. Characterisation of aged black carbon using pyrolysis-GC/MS, thermally assisted hydrolysis and methylation (THM), direct and cross-polarisation ^{13}C nuclear magnetic resonance (DP/CP NMR) and the benzenepolycarboxylic acid (BPCA) method. Org. Geochem. 39:1415–1426. doi:10.1016/j.orggeochem.2008.06.011

Karhu, K., T. Mattila, I. Bergstrom, and K. Regina. 2011. Biochar addition to agricultural soil increased CH_4 uptake and water holding capacity: Results

from a short-term pilot field study. Agric. Ecosyst. Environ. 140:309–314. doi:10.1016/j.agee.2010.12.005

Kilcoyne, A.L.D., T. Tyliszczak, W.F. Steele, S. Fakra, P. Hitchcock, K. Franck, et al. 2003. Interferometer-controlled scanning transmission X-ray microscopes at the Advanced Light Source. J. Synchrotron Radiat. 10:125–136. doi:10.1107/S0909049502017739

Kim, P., A. Johnson, C.W. Edmunds, M. Radosevich, F. Vogt, T.G. Rials, and N. Labbé. 2011. Surface functionality and carbon structures in lignocellulosic-derived biochars produced by fast pyrolysis. Energy Fuels 25:4693–4703. doi:10.1021/ef200915s

Kinyangi, J., D. Solomon, B. Liang, M. Lerotic, S. Wirick, and J. Lehmann. 2006. Nanoscale biogeocomplexity of the organomineral assemblage in soil. Soil Sci. Soc. Am. J. 70:1708–1718. doi:10.2136/sssaj2005.0351

Kloss, S., F. Zehetner, A. Dellantonio, R. Hamid, F. Ottner, V. Liedtke, et al. 2012. Characterization of slow pyrolysis biochars: Effects of feedstocks and pyrolysis temperature on biochar properties. J. Environ. Qual. 41:990–1000. doi:10.2134/jeq2011.0070

Lehmann, J., C.I. Czimczik, D.L. Laird, and S. Sohi. 2009. Stability of biochar in soil. In: J. Lehmann and S. Joseph, editors, Biochar for environmental management: Science and technology. Earthscan, London. p. 183–206.

Lehmann, J., and S. Joseph, editors. 2009. Biochar for environmental management: Science and technology. Earthscan, London.

Lehmann, J., B. Liang, D. Solomon, M. Lerotic, F. Luizao, J. Kinyangi, et al. 2005. Near-edge X-ray absorption fine structure (NEXAFS) spectroscopy for mapping nano-scale distribution of organic carbon forms in soil: Application to black carbon particles. Global Biogeochem. Cycles 19:GB1013. doi:10.1029/2004gb002435

Lehmann, J., and D. Solomon. 2010. Organic carbon chemistry in soils observed by synchrotron-based spectroscopy. In: S. Balwant and G. Markus, editors, Synchrotron-based techniques in soils and sediments. Dev. Soil Sci. 34. Elsevier, Amsterdam. p. 289–312.

Liang, B., J. Lehmann, D. Solomon, J. Kinyangi, J. Grossman, B. O'Neill, et al. 2006. Black carbon increases cation exchange capacity in soils. Soil Sci. Soc. Am. J. 70:1719–1730. doi:10.2136/sssaj2005.0383

Lin, Y., P. Munroe, S. Joseph, S. Kimber, and L. Zwieten. 2012. Nanoscale organo-mineral reactions of biochars in ferrosol: An investigation using microscopy. Plant Soil 357:369–380. doi:10.1007/s11104-012-1169-8

Liu, Y., M. Yang, Y. Wu, H. Wang, Y. Chen, and W. Wu. 2011. Reducing CH_4 and CO_2 emissions from waterlogged paddy soil with biochar. J. Soils Sediments 11:930–939. doi:10.1007/s11368-011-0376-x

Lovley, D.C., J. Blunt-Harris, E. Phillips, and J. Woodward. 1996. Humic substances as electron acceptors for microbial respiration. Nature 382:445–448. doi:10.1038/382445a0

Major, J., M. Rondon, D. Molina, S. Riha, and J. Lehmann. 2010. Maize yield and nutrition during 4 years after biochar application to a Colombian savanna Oxisol. Plant Soil 333:117–128. doi:10.1007/s11104-010-0327-0

McBeath, A.V., and R.J. Smernik. 2009. Variation in the degree of aromatic condensation of chars. Org. Geochem. 40:1161–1168. doi:10.1016/j.orggeochem.2009.09.006

Middelburg, J.J. 1989. A simple rate model for organic matter decomposition in marine sediments. Geochim. Cosmochim. Acta 53:1577–1581. doi:10.1016/0016-7037(89)90239-1

Moffet, R.C., A.V. Tivanski, and M.K. Gilles. 2010. Scanning transmission X-ray microscopy: Applications in atmospheric aerosol research. In: R. Signorell and J.P. Reid, editors, Fundamentals and applications in aerosol spectroscopy. CRC Press, Boca Raton, FL. p. 419–462.

Mukome, F.N.D., J. Six, and S.J. Parikh. 2013a. The effects of walnut shell and wood feedstock biochar amendments on greenhouse gas emissions from a fertile soil. Geoderma 200–201:90–98. doi:10.1016/j.geoderma.2013.02.004

Mukome, F.N.D., X. Zhang, L.C.R. Silva, J. Six, and S.J. Parikh. 2013b. Use of chemical and physical characteristics to investigate trends in biochar feedstocks. J. Agric. Food Chem. 61:2196–2204. doi:10.1021/jf3049142

Ravel, B., and M. Newville. 2005. ATHENA, ARTEMIS, HEPHAESTUS: Data analysis for X-ray absorption spectroscopy using IFEFFIT. J. Synchrotron Rad. 12:537–541. doi:10.1107/S0909049505012719

Schafer, T., N. Hertkorn, R. Artinger, F. Claret, and A. Bauer. 2003. Functional group analysis of natural organic colloids and clay association kinetics using C(1s) spectromicroscopy. J. Phys. IV 104:409–412.

Scheinost, A.C., R. Kretzschmar, I. Christl, and C. Jacobsen. 2001. Carbon group chemistry of humic and fulvic acid: A comparison of C-1s NEXAFS and ^{13}C-NMR spectroscopies. In: E.A. Gabbour and G. Davies, editors, Humic substances: Structures, models and functions. Spec. Publ. 273. R. Soc. Chem., Cambridge, UK. p. 39–47.

Scott, D.T., D.M. McKnight, E.L. Blunt-Harris, S.E. Kolesar, and D.R. Lovley. 1998. Quinone moieties act as electron acceptors in the reduction of humic substances by humics-reducing microorganisms. Environ. Sci. Technol. 32:2984–2989. doi:10.1021/es980272q

Shafizadeh, F., and Y. Sekiguchi. 1984. Oxidation of chars during smoldering combustion of cellulosic materials. Combust. Flame 55:171–179. doi:10.1016/0010-2180(84)90025-7.

Skjernstad, J.O., J.A. Taylor, and R.J. Smernik. 1999. Estimation of charcoal (char) in soils. Commun. Soil Sci. Plant Anal. 30:2283–2298. doi:10.1080/00103629909370372

Solomon, D., J. Lehmann, J. Kinyangi, B. Liang, K. Heymann, L. Dathe, et al. 2009. Carbon (1s) NEXAFS spectroscopy of biogeochemically relevant reference organic compounds. Soil Sci. Soc. Am. J. 73:1817–1830. doi:10.2136/sssaj2008.0228

Solomon, D., J. Lehmann, J. Kinyangi, B.Q. Liang, and T. Schafer. 2005. Carbon K-edge NEXAFS and FTIR-ATR spectroscopic investigation of organic carbon speciation in soils. Soil Sci. Soc. Am. J. 69:107–119. doi:10.2136/sssaj2005.0107dup

Solomon, D., J. Lehmann, J. Wang, J. Kinyangi, K. Heymann, Y. Lu, et al. 2012. Micro- and nano-environments of C sequestration in soil: A multi-elemental STXM–NEXAFS assessment of black C and organomineral associations. Sci. Total Environ. 438:372–388. doi:10.1016/j.scitotenv.2012.08.071

Spokas, K.A., W.C. Koskinen, J.M. Baker, and D.C. Reicosky. 2009. Impacts of woodchip biochar additions on greenhouse gas production and sorption/degradation of two herbicides in a Minnesota soil. Chemosphere 77:574–581. doi:10.1016/j.chemosphere.2009.06.053

Spokas, K.A., J.M. Novak, C.E. Stewart, K.B. Cantrell, M. Uchimiya, M.G. DuSaire, and K.S. Ro. 2011. Qualitative analysis of volatile organic compounds on biochar. Chemosphere 85:869–882. doi:10.1016/j.chemosphere.2011.06.108

Stevenson, F.J. 1994. Humus chemistry: Genesis, composition, reactions. 2nd ed. John Wiley & Sons, New York.

Stöhr, J. 1992. NEXAFS spectroscopy. Springer Ser. Surf. Sci. 25. Springer-Verlag, Berlin.

Uchimiya, M., I.M. Lima, K.T. Klasson, and L.H. Wartelle. 2010. Contaminant immobilization and nutrient release by biochar soil amendment: Roles of natural organic matter. Chemosphere 80:935–940. doi:10.1016/j.chemosphere.2010.05.020

Van Zwieten, L., S. Kimber, S. Morris, K. Chan, A. Downie, J. Rust, et al. 2010. Effects of biochar from slow pyrolysis of papermill waste on agronomic performance and soil fertility. Plant Soil 327:235–246. doi:10.1007/s11104-009-0050-x

Yao, F.X., M.C. Arbestain, S. Virgel, F. Blanco, J. Arostegui, J.A. Maciá-Agulló, and F. Macías. 2010. Simulated geochemical weathering of a mineral ash-rich biochar in a modified Soxhlet reactor. Chemosphere 80:724–732. doi:10.1016/j.chemosphere.2010.05.026

Yu, P., J.J. McKinnon, C.R. Christensen, and D.A. Christensen. 2004. Using synchrotron transmission FTIR microspectroscopy as a rapid, direct, and nondestructive analytical technique to reveal molecular microstructural–chemical features within tissue in grain barley. J. Agric. Food Chem. 52:1484–1494. doi:10.1021/jf035065a

Zimmerman, A.R. 2010. Abiotic and microbial oxidation of laboratory-produced black carbon (biochar). Environ. Sci. Technol. 44:1295–1301. doi:10.1021/es903140c

Zimmerman, A.R., B. Gao, and M.-Y. Ahn. 2011. Positive and negative carbon mineralization priming effects among a variety of biochar-amended soils. Soil Biol. Biochem. 43:1169–1179. doi:10.1016/j.soilbio.2011.02.005